

Improved resolution in fluorescence microscopy using quantum correlations

O. Schwartz and D. Oron

Department of Physics of Complex Systems, Weizmann Institute of Science, IL-76100 Rehovot, Israel

(Received 14 April 2011; published 16 March 2012)

Breaking the diffraction limit in microscopy by utilizing the quantum properties of light has been the goal of intense research in recent years. We propose a super-resolution technique based on nonclassical emission statistics of fluorescent markers, routinely used as contrast labels for bioimaging. The technique can be readily implemented with current technology.

DOI: [10.1103/PhysRevA.85.033812](https://doi.org/10.1103/PhysRevA.85.033812)

PACS number(s): 42.50.-p, 42.30.-d

I. INTRODUCTION

Increasing the imaging resolution in optical microscopy can potentially benefit many fields of research, including the life sciences. In classical linear optics, diffraction imposes a limit on the resolution of far-field microscopy. In the last two decades, a number of techniques have been developed that break this limit by making use of nonlinear optical processes [1–3] or by utilizing fluorescent labels exhibiting strong variations in brightness either induced by photoactivation [4–6] or intrinsic [7,8].

Quantum optics offers another promising pathway to super-resolution imaging. Quantum optical methods have been shown to dramatically increase the resolution in interferometric measurements [9] and allow for imaging-sensitivity enhancement beyond shot noise [10]. At the same time, super-resolution via quantum imaging has not yet been demonstrated experimentally. The theoretical research aiming at achieving subdiffraction-limited quantum imaging has mainly focused on the scenario wherein an absorptive object is illuminated with a nonclassical light beam. Super-resolution is then attained via two main routes. One requires an object stained with a multiphoton absorbing material. In this scheme, the diffraction limit is overcome by utilizing the high-spatial-frequency quantum interference patterns, similar to quantum super-resolution lithography [11]. Although multiphoton interference patterns of high order have been observed experimentally using coincidence detection [12–14], the lack of a low-light-level multiphoton absorber makes this approach not currently feasible. The other pathway to achieving subdiffraction resolution is probing an object with a beam of light exhibiting position (or momentum) entanglement. The high-resolution images can then be obtained simply by coincidence detection [15,16]. Although momentum-entangled light can be produced by spontaneous parametric down-conversion [17,18], the resolution in this case is limited by the diffraction limit at the pumping wavelength. Increasing the resolution further requires a bright, highly entangled light source, which has yet to be developed.

The above super-resolution schemes exploit quantum properties of the illuminating light and thus require nonclassical light sources. Alternatively, one can image emitters naturally producing nonclassical light, e.g., correlated photon pairs [19,20]. However, due to the lack of a suitable emitter, this approach has not been tested experimentally. It was also shown theoretically [21] that resonant fluorescence can produce multiphoton interference patterns which can be used for super-

resolved imaging of the emitters. While this approach can be feasible for imaging trapped ions, its reliance on fragile quantum effects makes it impractical for bioimaging conditions.

In this paper, we consider a generic property of fluorescence emitters: photon antibunching [22], arising from the tendency of fluorophores to emit photons one by one rather than in bursts. Antibunching is a distinctively quantum phenomenon, implying reduced quantum fluctuations (squeezing) of light [23] and sub-Poissonian photon statistics [24]. On the other hand, it is a very robust effect, exhibited by various fluorophores at room temperature [25–27]. Antibunching has become a standard tool for determining the number of fluorescent emitters [28]; however, it has not been utilized for resolution enhancement. We study the nonclassical photon statistics of fluorescence in connection to fluorescence microscopy and show that it can be used for super-resolved microscopic imaging under realistic conditions.

II. RESULTS

For simplicity, we focus on the case of pulsed excitation with the pulse duration much shorter and the interval between pulses much longer than the fluorescence lifetime. Upon excitation, a single fluorophore emits at most one photon with a probability p . In other words, the number N of photons emitted following a single excitation pulse follows a Bernoulli distribution with parameter p . Such behavior is profoundly different from the Poissonian statistics of classical light. In particular, the variance of the number of fluorescent photons emitted following a single excitation pulse is $V = p(1 - p)$ while the mean photon number is $\langle N \rangle = p$. A classical light source with the same photon flux would yield a variance $V_p = \langle N \rangle$. The variance of the fluorescent-photon number is thus reduced by a factor of $(1 - p)$ with respect to the classical shot noise, corresponding to a negative value of the Mandel parameter $Q = -p$ [29].

The nonclassical statistics of fluorescent light can be used to produce super-resolved images of fluorophores. Consider a fluorescent emitter, imaged by a microscopic imaging system onto a pixelated (or scanning) detector with photon-number-resolving capability. At every detector position x , the probability $P(x)$ to detect a photon emitted by the fluorophore is given by

$$P(x) = pGSh(x - x_0), \quad (1)$$

where G is the quantum efficiency of the detector, S denotes the optical collection efficiency, h is the point spread function of

the imaging system, and x_0 describes the coordinates of the fluorophore image. The photon-number variance becomes a function of the detector position $V(x) = P(x)[1 - P(x)]$. For a set of several fluorophores, since the emission events in different fluorophores are uncorrelated, the variance of the total photon number is given by the sum of variances for every emitter:

$$V(x) = \sum_{\alpha} P_{\alpha}(x)[1 - P_{\alpha}(x)], \quad (2)$$

where P_{α} is the photon-detection probability of the fluorophore α .

The difference between Eq. (2) and the classical shot noise variance at the same mean flux quantifies the degree of antibunching of fluorescent light and can therefore be called the antibunching signal

$$A(x) \equiv V(x) - \langle N(x) \rangle = -G^2 S^2 \sum_{\alpha} p_{\alpha}^2 h^2(x - x_{\alpha}). \quad (3)$$

The antibunching signal (3) can also be expressed as

$$A(x) = [g^{(2)}(0) - 1] \langle N(x) \rangle^2 = Q(x) \langle N(x) \rangle, \quad (4)$$

where $g^{(2)}(\tau) = \langle a^{\dagger}(0)a^{\dagger}(\tau)a(\tau)a(0) \rangle / \langle a^{\dagger}a \rangle^2$ is the second-order intensity-correlation function [29] and $Q(x)$ is the Mandel parameter observed at a given detector location. The signal $A(x)$, defined here in terms of the number of fluorescence photons detected after a single excitation pulse, can be accumulated over an arbitrary number of excitation cycles. This signal corresponds to an effective point spread function $h_A(x) = h^2(x)$. In the Fourier domain, h_A spans an interval of spatial frequencies twice as large as that of h . The antibunching microscopy thus enables imaging with up to double resolution, similar to the resolution improvement (relative to the wavelength) attainable with two-photon microscopy [30].

The mechanism of the antibunching microscopy is illustrated in Fig. 1 for the case of two identical emitters. The

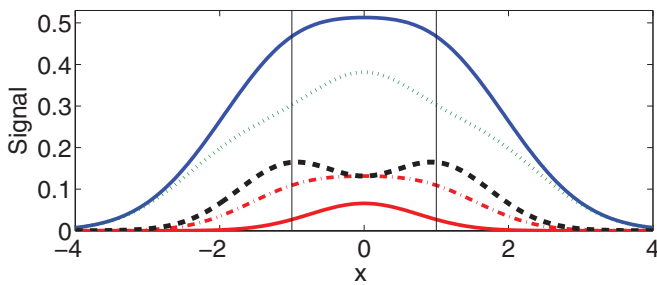


FIG. 1. (Color online) Image plane signal distribution for antibunching imaging of two fluorescent emitters. The units are arbitrary in both axes. The vertical lines denote the locations of the emitters. The solid blue line (top curve) is the regular fluorescent signal as a function of the image plane coordinate x , the dotted green line represents the variance given by Eq. (2), the dashed black line is the antibunching signal (3). The solid red line (bottom curve) shows the probability $F_2(x) = P_1(x)P_2(x)$ of a two-photon coincidence event with a sharp peak in the center. The dash-dotted red line shows the two-photon probability for two classical emitters $F_2^c(x) = (P_1(x) + P_2(x))^2/2$, featuring a wider peak. The plots are calculated for $P_1(x-1) = P_2(x+1) = 0.4 \exp(-x^2/2.25)$.

emitters are not resolved in the fluorescent signal while two separate peaks are visible in the antibunching signal. It is instructive to consider photon statistics in the limit of small photon flux. Let $F_1(x)$ and $F_2(x)$ be the probabilities of detecting exactly one and two photons, respectively, at a given detector position. We assume here $F_2 \ll F_1 \ll 1$ and neglect the probability of detecting more than two photons. In terms of these probabilities, the average photon number and the variance become $\langle N \rangle = [F_1(x) + 2F_2(x)]$ and $V(x) \simeq (F_1 + 4F_2 - F_1^2)$, respectively. The antibunching signal (3) then takes the form of $A(x) \simeq [2F_2(x) - F_1^2(x)]$. Since this expression vanishes for Poissonian statistics, the antibunching signal can be regarded as a measure of the lack of two-photon coincidence events with respect to classical light.

This observation elucidates the mechanism of the resolution increase shown in Fig. 1. In this example, a coincidence event involves the detection of one photon from each of the fluorophores. The probability of a coincidence event therefore has a sharp maximum positioned between the two emitters. This is in contrast to the case of two classical emitters for which a pair of photons could as well originate from a single emitter, making the maximum less sharp.

The antibunching signal (3) is determined by the optical-signal autocorrelation at a given detector position. Fluorescence antibunching is also manifest in the cross correlation between the photon numbers $N(x_1)$ and $N(x_2)$ detected in a pair of proximate detectors. Similar to variance, the covariance of the two signals $V^{\times}(x_1, x_2) = \langle N(x_1)N(x_2) \rangle - \langle N(x_1) \rangle \langle N(x_2) \rangle$ is a sum of individual fluorophore contributions. For classical light, the signals observed in the detectors are uncorrelated, and therefore, covariance vanishes. In contrast, an individual fluorophore produces only one photon at a time, which can be detected in only one of the detectors, leading to $N(x_1)N(x_2) = 0$. The covariance antibunching signal can thus be defined as

$$A^{\times}(x_1, x_2) = \sum_{\alpha} V_{\alpha}^{\times}(x_1, x_2) = - \sum_{\alpha} P_{\alpha}(x_1)P_{\alpha}(x_2), \quad (5)$$

where x_1 and x_2 are the detector positions and $P_{\alpha}^{(1)}$ and $P_{\alpha}^{(2)}$ are the detection probabilities for a given fluorophore at the two detectors. The antibunching signal (5) contains a product of two optical point spread functions. As we show below, it can be used to produce higher-resolution images along with the autocorrelation antibunching signal of Eq. (3).

We numerically tested the resolution improvement in antibunching microscopy by performing a Monte Carlo simulation of the antibunching-imaging process using a pixelated detector array. For efficient signal utilization, we used both the autocorrelation antibunching signal of Eq. (3) and the cross-correlation data of Eq. (5) to form the image. The autocorrelation antibunching signal at a given pixel, numbered by a two-dimensional index j , is given by

$$A_j = \sum_{\alpha} P_{\alpha}(j)^2 = V_j - \langle N_j \rangle, \quad (6)$$

where $\langle N_j \rangle$ is the mean number of photons and V_j is the variance of the photon number. The cross-correlation contribution to the second-order antibunching signal was calculated as a weighted sum of the cross correlations of the pairs of pixels $j \pm \delta$, centered at the pixel j . The simulation was

carried out as follows. A stack of 10^5 frames was generated, each representing a fluorescence image obtained following a single excitation pulse. One photon from every fluorophore was placed randomly with a probability density corresponding to a Gaussian point spread function with a total probability to emit of 0.5. The resulting stack of single-exposure images was used to compute the second-order antibunching signal according to the following formula:

$$A_j = \sum_{\delta} W(\delta) (\langle N_{j+\delta} N_{j-\delta} \rangle - \langle N_{j+\delta} \rangle \langle N_{j-\delta} \rangle) - \langle N_j \rangle, \quad (7)$$

where N_j is the number of photons detected in the pixel j ; δ is a summation index labeling the pixel pairs, running from -6 to 6 in both dimensions; $W(\delta) = \exp[-0.033\delta^2]$ is the weight assigned to the pixel pairs; and the angular brackets denote averaging over the set of frames.

The above analysis does not fully utilize the cross-correlation information. Indeed, only a half of all pixel pairs are centered in a certain pixel. A pair of, for example, two adjacent pixels has its center between the two pixels. It is therefore possible to compute the antibunching signal in “virtual pixels” in between adjacent pixels, i.e., with at least one of the two components of j being a half-integer [31]. The effective number of pixels in each direction is thus doubled, increasing the total amount of pixels by a factor of four. The signal in the virtual pixels was calculated using Eq. (7) with the last term omitted and with one or both components of the summation index δ assuming half-integer values (so that $i \pm \delta$ are integers). The results of the simulation shown in Fig. 2 demonstrate a significant improvement of resolution. The individual emitters, which cannot be discerned by regular imaging, are clearly resolved in the antibunching image.

The antibunching signal, defined above in terms of second-order momenta, serves as a measure of the lack of two-photon coincidence events. Hence, it can be called the second-order antibunching signal. The n th order antibunching signal $A_n(x)$, quantifying the lack of n -photon events, can be defined in terms of the irreducible parts of the n th-order momenta known as cumulants [32]

$$C_n = \left[\left(\frac{\partial}{\partial t} \right)^n \ln \langle \exp(Nt) \rangle \right]_{t=0}. \quad (8)$$

The defining property of cumulants is that they are additive for independent random variables, allowing one to express the

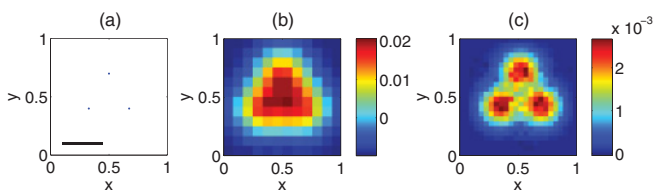


FIG. 2. (Color online) A simulation of the second-order antibunching imaging. (a) Three emitters are positioned in the vertices of an equilateral triangle. The units are arbitrary, and the scale bar shows the full width at half maximum of the optical-point-spread function. (b) The regular fluorescence image does not resolve the emitters. (c) The second-order antibunching image. The emitters are clearly discerned. Both images were formed from 10^5 frames, each corresponding to a single excitation cycle.

cumulants of the observed signal as a sum of the individual fluorophore contributions. For a single fluorophore, the n th-order cumulant is given by $C_n = P(1 - P) \cdots [1 - (n - 1)P]$. The cumulants $C_n(x)$ of the total signal are therefore given by

$$C_n(x) = \sum_{\alpha} P_{\alpha}(x) [1 - P_{\alpha}(x)] \cdots [1 - (n - 1)P_{\alpha}(x)]. \quad (9)$$

The antibunching signal of order n can then be defined as

$$A_n(x) = \sum_{\alpha} P_{\alpha}^n(x), \quad (10)$$

which can be expressed via cumulants of order $k \leq n$ using Eq. (9):

$$A_n(x) = \sum_k (\hat{R}^n)_{1k} C_k(x), \quad (11)$$

where $(\hat{R}^n)_{1k}$ is the first row of the n th power of a matrix \hat{R} , all elements of which are zero except

$$R_{kk} = -R_{k-1k} = 1/k. \quad (12)$$

The signals $A_n(x)$ vanish in the classical limit and are therefore a valid local measure of the degree of antibunching. For $n = 2$, the above expressions yield the second-order antibunching signal described above. Substituting Eq. (1) into the definition (10), one obtains

$$A_n(x) = G^n S^n \sum_{\alpha} p_{\alpha}^n [h(x - x_i)]^n. \quad (13)$$

Effectively, the n th-order antibunching signal corresponds to a point-spread function $h_n(x) = [h(x)]^n$. Similar to the second order, this enables imaging with resolution up to n times better than that of diffraction-limited imaging in three dimensions [3,30].

III. DISCUSSION

Quantum-fluorescence imaging requires fluorophores with as high quantum yields as possible. Fortunately, many of the fluorescent markers widely used in bioimaging, such as organic dyes, have quantum yields approaching unity. Very high quantum yields have also been demonstrated with colloidal semiconductor quantum dots [33].

Many fluorescent single-photon emitters exhibit random variations of brightness known as blinking. Blinking increases the observed photon-number fluctuations and could be expected to change the photon statistics to super-Poissonian. It turns out, however, not to be the case. Indeed, for a single emitter, the photon number follows a Bernoulli distribution even in the presence of blinking, the only consequence of which is an effective reduction of the emission probability. As long as the blinking of individual fluorophores is uncorrelated, the antibunching properties of emission statistics persist for an arbitrary number of emitters.

The photon-number distributions required for computing the cumulants in Eq. (11) can be determined with a scanning number resolving detector [34,35]. Another option is using a regular or an electron-multiplying charged coupled device (ccd) [16]. An electron-multiplying ccd in the photon-counting regime can be used as a pixelated number resolving detector, provided that the number of pixels is sufficiently large so that

the probability of detecting more than one photon in a pixel is small. Both the scanning number resolving detectors and ccds can achieve quantum yields in excess of 90% [34,36].

The acquisition times necessary to obtain sufficient photon statistics can potentially be very short. Since most fluorophores have relaxation times in the nanosecond range, the antibunched photons can be collected at a rate of at least a few tens of millions of excitation pulses per second. The speed of data acquisition, however, is currently limited by the detector throughput. The future progress of detector technology may eliminate this bottleneck through the development of faster electron-multiplying cameras [37] or larger single-photon-detector arrays [38]. With a sufficiently fast detector, antibunching microscopy can enable super-resolved imaging at millisecond time scales.

Antibunching microscopy can be regarded as a quantum version of super-resolution optical-fluctuation imaging (SOFI) [8]. In this technique, the n th-order signal is given by the n th cumulant without the lower-order “correction” terms appearing in Eq. (11). Interestingly, the antibunching signal vanishes in the classical limit instead of turning into the corresponding SOFI expression. This is the case because the two schemes exploit different sources of non-Poissonian statistics. While

SOFI quantifies the super-Poissonian brightness fluctuations of essentially classical sources, in the present scheme the signal is due to the reduction of the quantum fluctuations with respect to the classical shot noise. The antibunching signal is thus generated by steadily emitting fluorophores, enabling continuous super-resolved monitoring of the samples stained with fluorescent markers.

In conclusion, we propose a fluorescence-microscopy-imaging modality that allows for subdiffraction-limited imaging by virtue of quantum properties of fluorescence emission. Despite being ostensibly quantum, the technique does not require a nonclassical light source and does not depend on fragile quantum-interference effects. The proposed method can be implemented with current technology or indeed with a regular fluorescence microscope.

ACKNOWLEDGMENTS

Support by the ERC Young Investigator Grant No. SINSILM 258221, the Israeli Ministry of Science “Tashtiyot” program, and the Crown Center of Photonics is gratefully acknowledged. O.S. is supported by the Adams Fellowship Program of the Israel Academy of Sciences and Humanities.

-
- [1] S. W. Hell and J. Wichmann, *Opt. Lett.* **19**, 780 (1994).
 [2] K. Fujita, M. Kobayashi, S. Kawano, M. Yamanaka, and S. Kawata, *Phys. Rev. Lett.* **99**, 228105 (2007).
 [3] M. G. L. Gustafsson, *Proc. Natl. Acad. Sci. USA* **102**, 13081 (2005).
 [4] E. Betzig, G. Patterson, R. Sougrat, O. Lindwasser, S. Olenych, J. Bonifacino, M. Davidson, J. Lippincott-Schwartz, and H. Hess, *Science* **313**, 1642 (2006).
 [5] S. T. Hess, T. P. K. Girirajan, and M. D. Mason, *Biophys. J.* **91**, 4258 (2006).
 [6] M. J. Rust, M. Bates, and X. Zhuang, *Nat. Methods* **3**, 793 (2006).
 [7] K. Lidke, B. Rieger, T. Jovin, and R. Heintzmann, *Opt. Express* **13**, 7052 (2005).
 [8] T. Dertinger, R. Colyer, G. Iyer, S. Weiss, and J. Enderlein, *Proc. Natl. Acad. Sci. USA* **106**, 22287 (2009).
 [9] V. Giovannetti, S. Lloyd, and L. Maccone, *Science* **306**, 1330 (2004).
 [10] G. Brida, M. Genovese, and I. R. Berchera, *Nat. Photonics* **4**, 227 (2010).
 [11] M. D’Angelo, M. V. Chekhova, and Y. Shih, *Phys. Rev. Lett.* **87**, 013602 (2001).
 [12] I. Afek, O. Ambar, and Y. Silberberg, *Science* **328**, 879 (2010).
 [13] P. Walther, J. Pan, M. Aspelmeyer, R. Ursin, S. Gasparoni, and A. Zeilinger, *Nature (London)* **429**, 158 (2004).
 [14] A. Pearlman, A. Ling, E. Goldschmidt, C. Wildfeuer, J. Fan, and A. Migdall, *Opt. Express* **18**, 6033 (2010).
 [15] V. Giovannetti, S. Lloyd, L. Maccone, and J. H. Shapiro, *Phys. Rev. A* **79**, 013827 (2009).
 [16] M. Tsang, *Phys. Rev. Lett.* **102**, 253601 (2009).
 [17] E. J. S. Fonseca, C. H. Monken, and S. Pádua, *Phys. Rev. Lett.* **82**, 2868 (1999).
 [18] W. A. T. Nogueira, S. P. Walborn, S. Pádua, and C. H. Monken, *Phys. Rev. Lett.* **86**, 4009 (2001).
 [19] S. W. Hell, J. Soukka, and P. E. Hänninen, *Bioimaging* **3**, 64 (1995).
 [20] A. Muthukrishnan, M. O. Scully, and M. S. Zubairy, *J. Opt. B: Quantum Semiclassical Opt.* **6**, S575 (2004).
 [21] C. Thiel, T. Bastin, J. Martin, E. Solano, J. von Zanthier, and G. S. Agarwal, *Phys. Rev. Lett.* **99**, 133603 (2007).
 [22] H. J. Kimble, M. Dagenais, and L. Mandel, *Phys. Rev. Lett.* **39**, 691 (1977).
 [23] D. F. Walls and P. Zoller, *Phys. Rev. Lett.* **47**, 709 (1981).
 [24] L. Mandel, *Opt. Lett.* **4**, 205 (1979).
 [25] W. Ambrose, P. Goodwin, J. Enderlein, D. Semin, J. Martin, and R. Keller, *Chem. Phys. Lett.* **269**, 365 (1997).
 [26] R. Brouri, A. Beveratos, J. Poizat, and P. Grangier, *Opt. Lett.* **25**, 1294 (2000).
 [27] B. Lounis, H. Bechtel, D. Gerion, P. Alivisatos, and W. Moerner, *Chem. Phys. Lett.* **329**, 399 (2000).
 [28] H. Ta, J. Wolfrum, and D. P. Herten, *Laser Phys.* **20**, 119 (2010).
 [29] L. Mandel and E. Wolf, *Rev. Mod. Phys.* **37**, 231 (1965).
 [30] O. Schwartz and D. Oron, *Opt. Lett.* **34**, 464 (2009).
 [31] T. Dertinger, R. Colyer, R. Vogel, J. Enderlein, and S. Weiss, *Opt. Express* **18**, 18875 (2010).
 [32] M. Kendall and A. Stuart, *The Advanced Theory of Statistics, Volume 1: Distribution Theory* (Griffin, London, 1977).
 [33] Y. Chen, J. Vela, H. Htoon, J. Casson, D. Werder, D. Bussian, V. Klimov, and J. Hollingsworth, *J. Am. Chem. Soc.* **130**, 5026 (2008).

- [34] A. E. Lita, A. J. Miller, and S. W. Nam, [Opt. Express](#) **16**, 3032 (2008).
- [35] F. Guerrieri, L. Maccone, F. N. C. Wong, J. H. Shapiro, S. Tisa, and F. Zappa, [Phys. Rev. Lett.](#) **105**, 163602 (2010).
- [36] C. G. Coates, D. J. Denvir, N. G. McHale, K. D. Thornbury, and M. A. Hollywood, [J. Biomed. Opt.](#) **9**, 1244 (2004).
- [37] P. Feautrier, J. Gach, P. Balard, C. Guillaume, M. Downing, N. Hubin, E. Stadler, Y. Magnard, M. Skegg, M. Robbins *et al.*, [Publications of the Astronomical Society of the Pacific](#) **123**, 263 (2011).
- [38] R. Colyer, G. Scalia, F. Villa, F. Guerrieri, S. Tisa, F. Zappa, S. Cova, S. Weiss, and X. Michalet, [Proceedings of SPIE](#) **7905**, 790503 (2011).